SI Appendix
Emergent Ultra-Long-Range Interactions Between Active Particles in Hybrid Active-Inactive Systems

I. SUPPLEMENTARY MATERIALS AND METHODS

A. Experimental Apparatus

To magnetically actuate and drive the spinners we developed the experimental apparatus seen in Fig. S1.

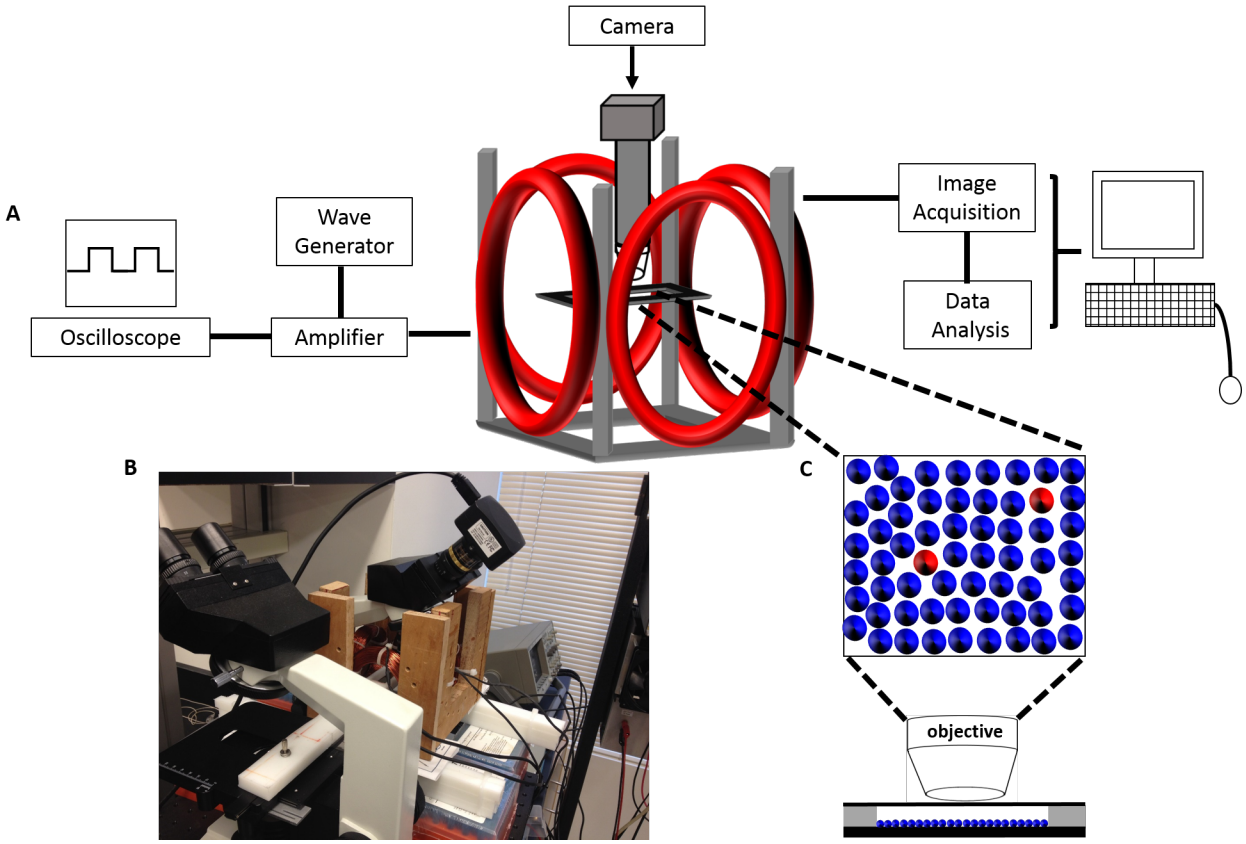

Fig. S 1. A)Schematic of experimental set-up. A light microscope was been mounted with four coils to produce an in plane rotating magnetic field. A wave generator ran two sinusoidal signals phase shifted by 90 degrees through an amplifier to generate a field strength of 5mT. An oscilloscope was used to monitor the frequency and a CCD camera mounted on the microscope was used to capture videos of the walker motion. B)Image of the experimental apparatus. C) The sample was placed at the center of the coils where the field is the most homogeneous. The solution of passive and active colloids in a surfactant solution was inserted into a microfluidic channel and sealed.

The apparatus consisted of two pairs of coils attached to a rectangular wooden box. The wooden box was mounted on a modified compound binocular light microscope (condenser lens, iris diaphragm, stage, and condenser focus all removed) provided by OMAX. Another OMAX microscope was modified so that it would act as a 3D mobile stage. The specimen clip was removed and a rectangular piece of nylon approximately 300mm×30mm was screwed into the mechanical stage and the sample was mounted on this piece of nylon (later the nylon was replaced by a wooden piece of similar dimensions). The box was then mounted so that the coils were centered on the sample holder. Two sinusoidal signals, phase shifted by 90 degrees, were generated by an external program, Audacity and/or MatLab,

and passed through each pair of coils (one signal per pair of coils). A 300W amplifier (150W/channel) ran 2.5 Amps through more than 100 turns of wire (in each coil) to obtain a field strength of approximately 5mT.

The magnitude of the field was calculated using the following equation

$$B(x,y) = \frac{INR^3\mu_o}{(R^2+(d_x-x)^2)^{\frac{3}{2}}} + \frac{INR^3\mu_o}{(R^2+(d_x+x)^2)^{\frac{3}{2}}} + \frac{INR^3\mu_o}{(R^2+(d_y-y)^2)^{\frac{3}{2}}} + \frac{INR^3\mu_o}{(R^2+(d_y+y)^2)^{\frac{3}{2}}} \quad (1)$$

where I is the current passed through the coils in Amperes, N is the number of turns of wire, R is the radius of the coils, μ_o is the magnetic constant, d_x is the distance between the two coils centered on the x-axis, and d_y is the distance between the two coils centered on the y-axis. The magnetic field strength across the apparatus can be seen in Fig. S2.

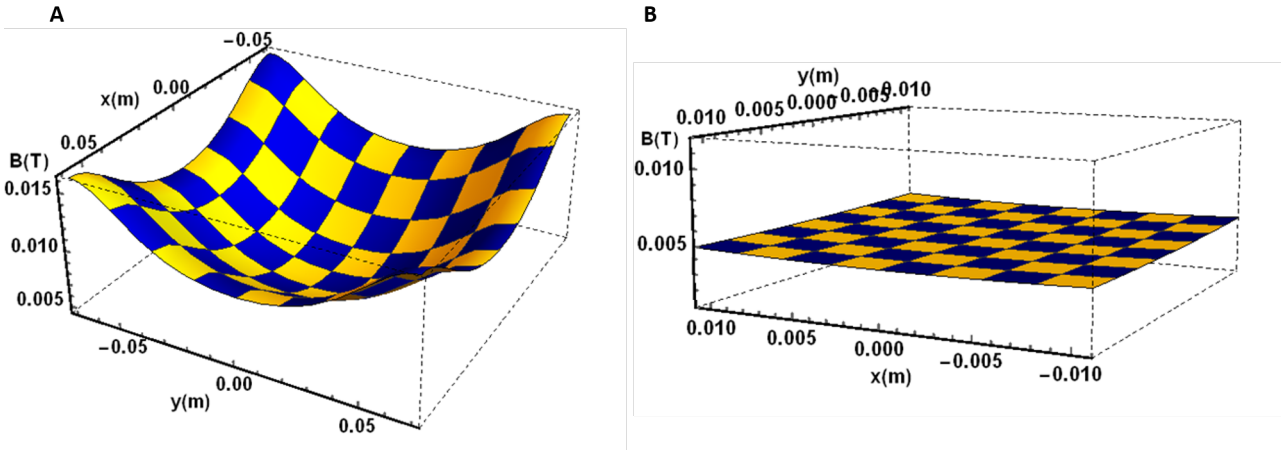

Fig. S 2. A) The magnetic field strength was plotted across the entire experimental apparatus. The magnetic of the field was largest at the center of each of the four coils. B) The magnetic field appears to be essentially homogeneous in the area of interest.

The magnetic field was largest at the center of each of the four coils and clearly across the entire apparatus the magnetic field is not homogeneous. But if we take a closer look at the area of interest, that is where the sample was placed, the field was essentially homogeneous with a field strength of approximately 5mT. The signal from the amplifier was routed to an oscilloscope, HP (Hewlett-Packard) H4601A, in order to get a precise measure of the frequency and the voltage at the output. Data acquisition was accomplished via a CCD camera that had been mounted on the microscope. The camera was connected to a computer for visualization, video capture, and subsequent analysis.

B. Spinner Sample Preparation in Purely Active and Passive Mediums

Ferromagnetic particles, approximately 5μm in diameter provided by Spherotech and henceforth referred to as spinners, were diluted to a concentration of approximately 2 μg/ml. The solution was vortexted for several minutes and then 10μL of this solution was inserted into a microfluidic channel. The channels were created using glass slides and strips of 3M double sided tape. Three pieces of tape were placed on top of each other and then small strips were cut and then placed on the slide to make rectangular channels of dimension 22×3mm. Once the solution was inserted, the channel was sealed with epoxy to prevent evaporation and evaporative induced flows. The slide was placed atop a neodymium magnet to magnetize the spinners and then moved to the sample holder. After several minutes, to allow for sedimentation, two spinners were isolated and the magnetic field was actuated for approximately five minutes or until the two spinners formed a dimer at a frequency of 0.5, 1, 3, and 5 Hz. Two isolated spinners actuated at a frequency of 5 Hz can be seen in the Movie S1, sped up 4×, in Fig. S3.

Additionally the distance between particles, R, normalized by the diameter, D, was measured as a function of time to investigate any potential attractive force felt between spinners. These trajectories can be seen in Fig. S4.

The trajectories show there was virtually no long range interaction between spinners in the absence of a dense passive medium at every frequency probed. Some spinners will form dimer within the experimental time period but only when the spinners were initially positioned close enough so that magnetic dipole-dipole interaction dominates,

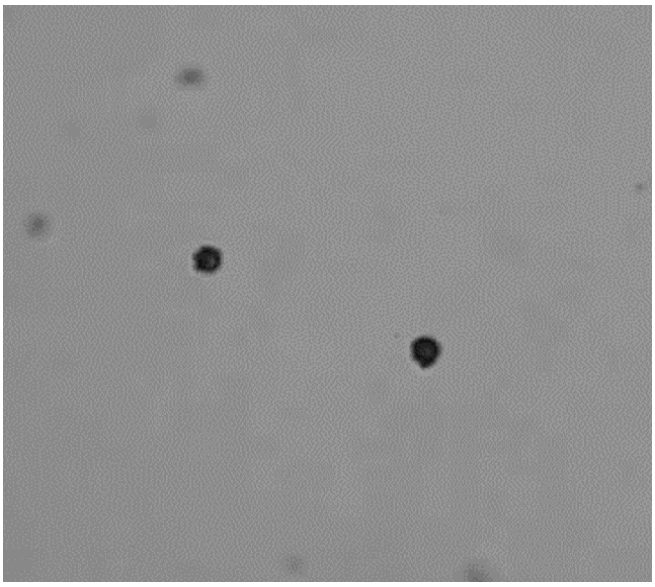

Fig. S 3. Two spinners in an extremely dilute purely active system actuated at a frequency of 5 Hz, sped up 4×. The spinners don't attract within the experimental time period.

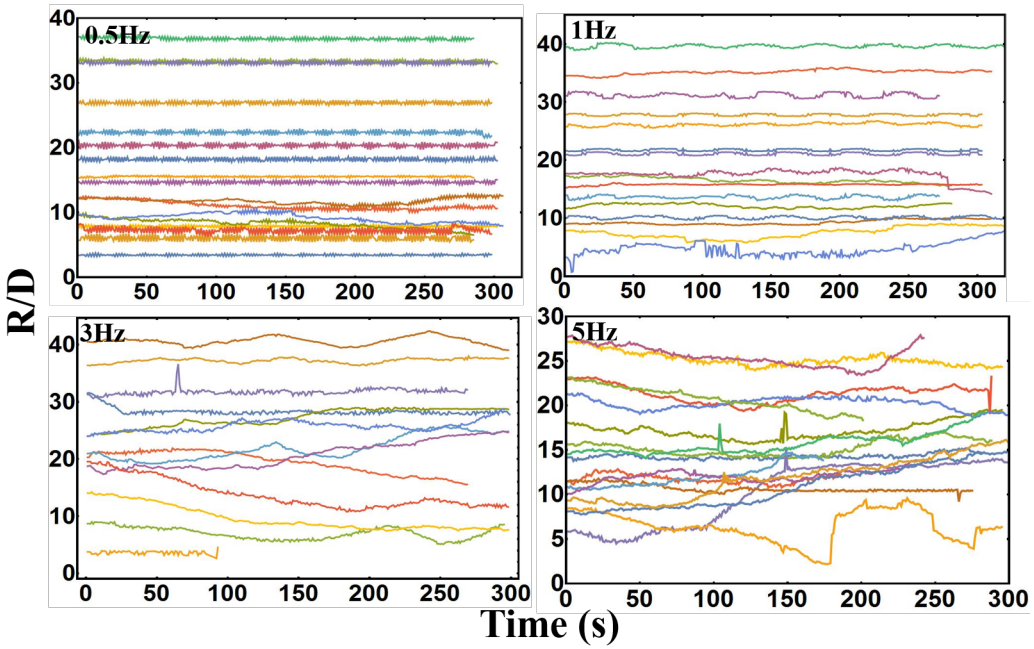

Fig. S 4. The distance between the spinners normalized by the diameter was plotted for spinners actuated at frequencies of 0.5, 1, 3, and 5 Hz. There was clearly no attractive force felt between the spinners unless the spinners were initially positioned a distance of approximately 3D or less.

which as described in the main text was experimentally determined to be approximately 3D for spinners actuated at approximately 5 Hz.

To investigate how spinner interaction changes when embedded in a dense passive medium. Ferromagnetic particles were again diluted to a concentration of 10 μg/mL and 10μL of this solution was mixed with 40μL of polystyrene particles, at a concentration of 10 mg/mL, approximately 5μm in diameter which was provided by Phosphorex. This solution was vortexted for several minutes and then 10μL was inserted into the microfluidic channel. The slide was placed atop a neodymium magnet to magnetize the spinners and then moved to the sample holder. After several minutes, to allow for sedimentation, the packing fraction was determined to be approximately 0.7. Two spinners were

isolated and the magnetic field was actuated for approximately five minutes or until the two spinners formed a dimer at a frequency of 0.5, 1, 3, and 5 Hz. Two spinners in a passive medium, $\phi_A \approx 0.7$, rotating at an angular frequency of 5 Hz can be seen in Movie S2, 4×, as seen in Fig. S5.

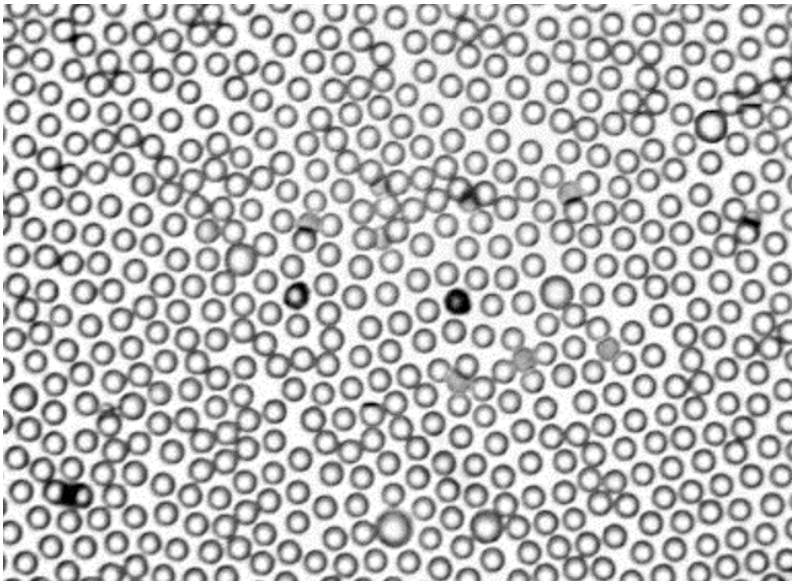

Fig. S 5. Two spinners in a passive medium, $\phi_A \approx 0.7$, actuated at a frequency of 5 Hz. The spinners form a dimer within the experimental time period. The video is sped up 4×.

The distance between particles, R, was measured as a function of time, and normalized by the particle diameter, to observe the attractive force between spinners, as seen in Fig. S6.

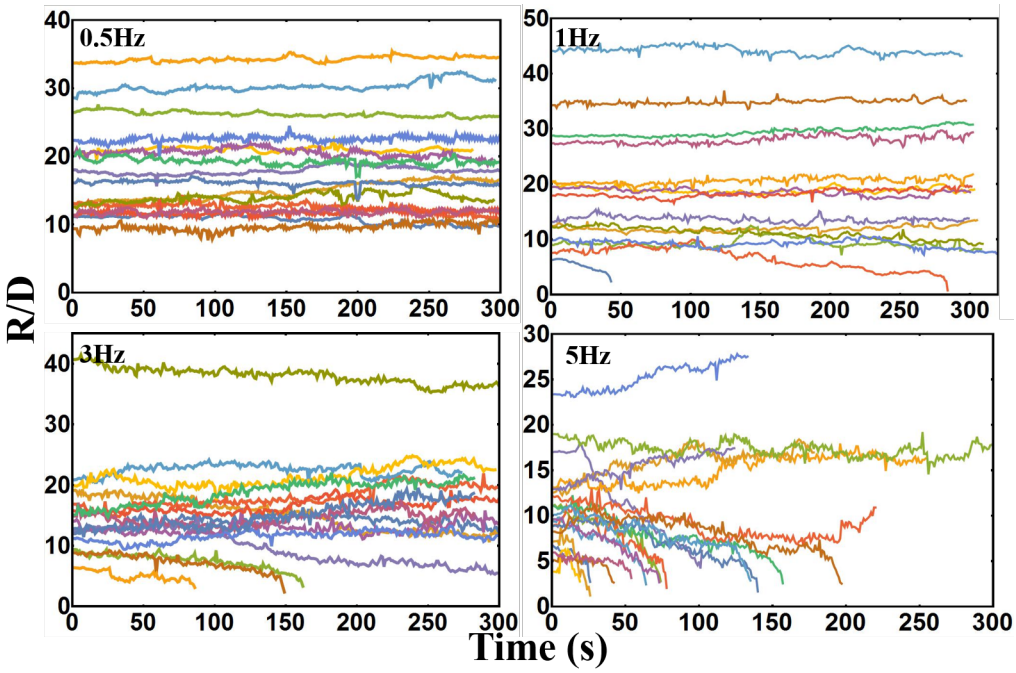

Fig. S 6. The normalized distance between spinners was plotted for 0.5, 1, 3, and 5 Hz. The interaction range increases with the angular frequency of rotation, reaching up to $17D$ for 5 Hz.

As explained in the manuscript there clearly seems to be a long range attractive force between the spinners and at 5 Hz the spinners are able to form a dimer at distances up to $17D$ apart.

C. Sample Preparation Varying Passive Medium Packing Fraction

To investigate the dependence of this long range attractive force on the concentration of the passive elastic medium the passive particle concentration was reduced until a packing fraction of approximately 0.5 and 0.3 was obtained, as seen in the images below in Fig. S7.

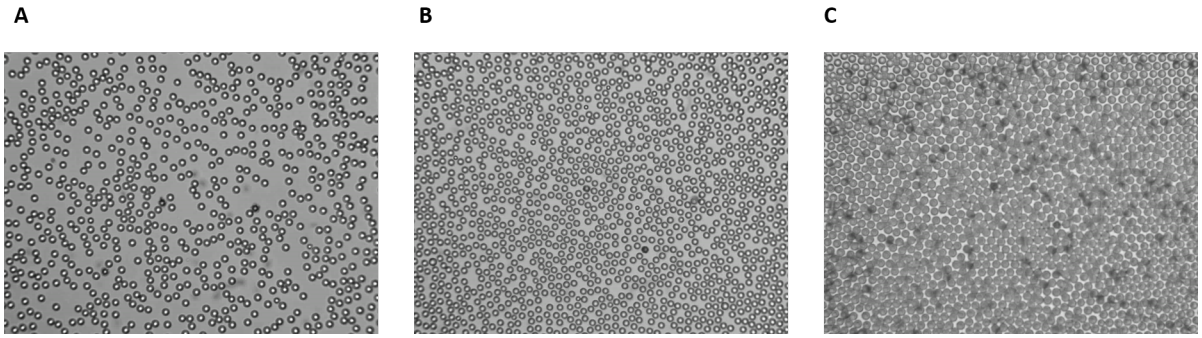

Fig. S 7. Images of spinners rotating in a passive medium with $\phi_A \approx$ A)0.3, B)0.5, and C)0.7

To achieve a packing fraction of approximately 0.5, 8μL of passive particles, at a concentration of 10 mg/mL, was mixed with 10μL of a solution of ferromagnetic particles at a concentration of 2μg/mL. A packing fraction of approximately 0.3 was achieved by mixing 5μL of passive particles, at a concentration of 5 mg/mL, with 10μL of ferromagnetic particles at a concentration of approximately 0.62 μg/mL. The slide was then placed again on the neodymium magnetic and moved to the sample holder and left for several minutes for sedimentation. Two spinners were then isolated and the magnetic field was actuated for approximately five minutes at 5 Hz or until the two spinners formed a dimer. The distance between particles, R, was measured as a function of time to measure the attractive force between spinners, as seen in Fig. S8.

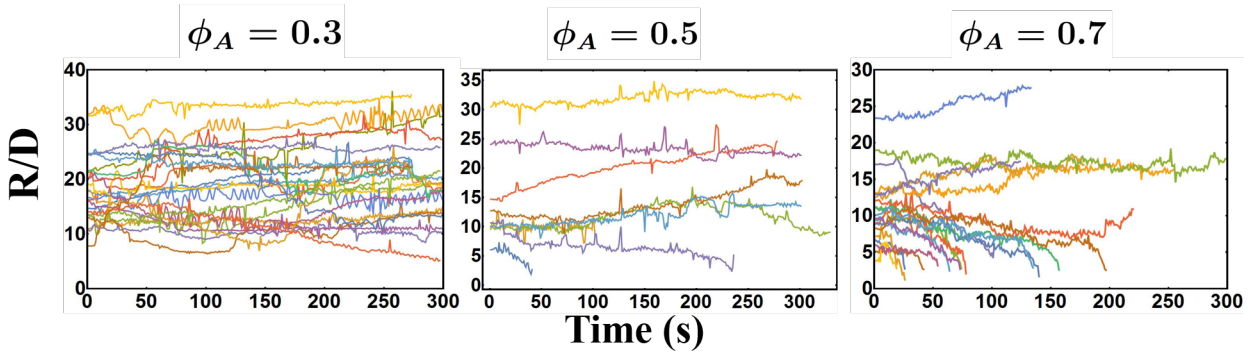

Fig. S 8. The normalized distance between the spinners in passive mediums with $\phi_A \approx 0.3, 0.5$, and 0.7. Long-range spinner attraction is lost at a packing fraction of approximately 0.3 and the range of attraction increases with the packing fraction.

It is clear that the long range attractive force has been lost when the packing fraction is reduced to 0.3. At this point the concentration of particles is so low that the medium no longer behaves elastically which we will confirm using passive microrheology, which will be discussed in the Passive Microrheology Measurements of Passive Medium Elasticity section.

D. Changing Relative Passive-Active Colloidal Sizes, Passive Colloidal Density, and Adding Strong Repulsive Potential Between Passive Particles

To ensure this behavior was somewhat ubiquitous and not unique to a passive medium composed of passive polystyrene particles we investigated spinner attraction in hybrid active-passive systems utilizing 9μm active particles and 5μm passive polystyrene particles, 5μm active particles and 3μm silica passive particles, and a 5μm active particles and 3μm silica passive particles with a strong repulsive potential. To create the system with 9μm active particles and 5μm passive polystyrene particles we doped a solution of 5μm passive particles, at a concentration of 8 mg/mL, with 9μm at a concentration of 5μg/mL and inserted the solution into the channel. The magnetic field was actuated at an angular frequency of 5 Hz as seen in the image in Fig. S9.

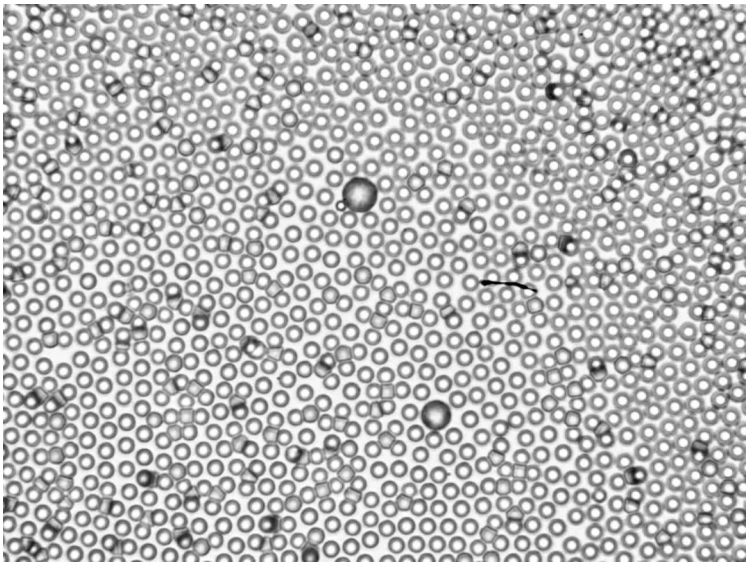

Fig. S 9. Image of 9μm active particle in a 5μm polystyrene passive medium.

The spinner binds and forms a dimer when initially positioned at approximately $17D$ apart, taking the diameter of the passive particles as D, as seen in Fig. S10.

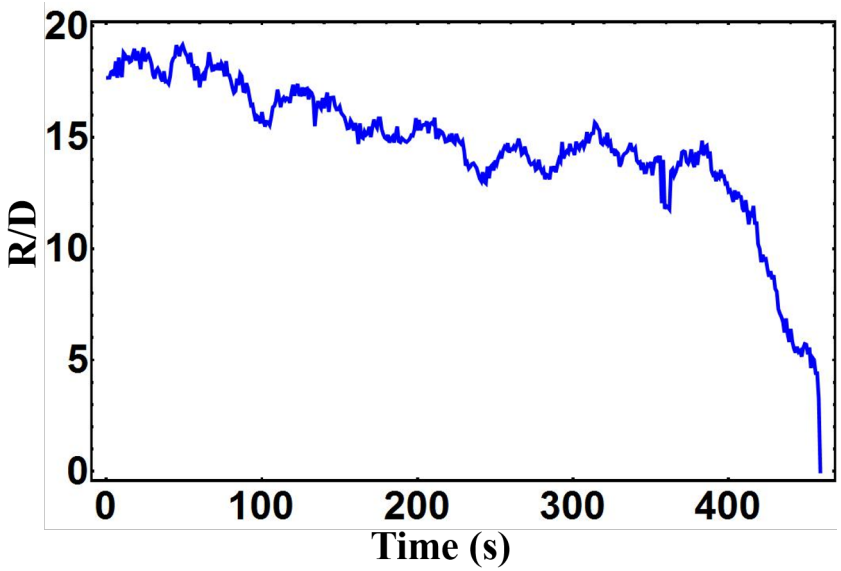

Fig. S 10. Spinners bind at extremely large initial distances in hybrid active-passive system with different sized active and passive particles composed of the same material

To create a system using 5μm active particles and 3μm silica passive particles we again mixed a dilute suspension of active particles, 3 μg/mL, with 3μm silica particles, at a concentration of 8 mg/mL. The magnetic field was actuated at an angular frequency of 5 Hz as seen in the image in Fig. S11.

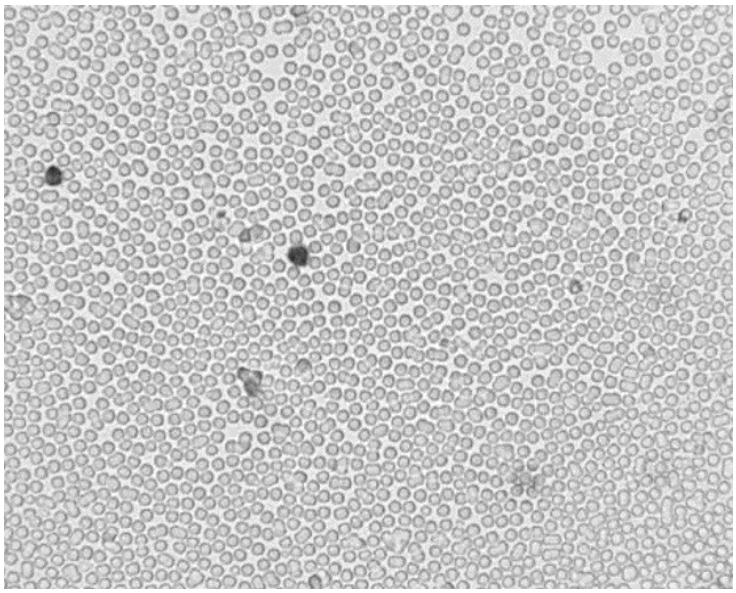

Fig. S 11. Image of 5μm active particle in a 3μm silica passive medium.

Looking at several pairs of spinners we see attraction up to 15D apart, again we normalize by the diameter of the passive particles, as seen in Fig. S12.

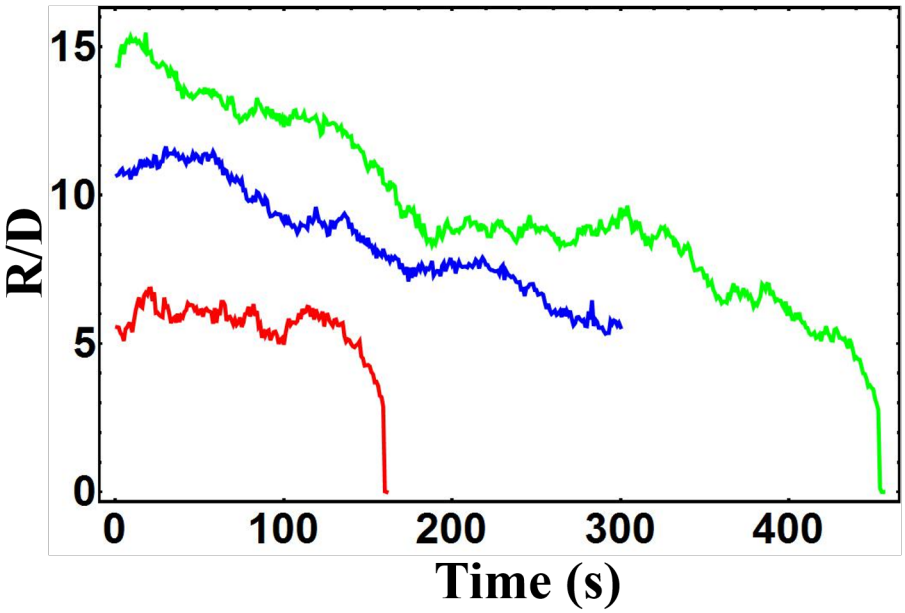

Fig. S 12. Spinner interaction range is again extremely long rage, up to 15D, for another hybrid active-passive system.

To create a system with 5μm active particles and 3μm silica passive particles with a strong repulsive potential we

polarized silica beads by establishing a voltage between two slides. To establish this voltage we used two ITO slides, 50 $\Omega/\square$, and create a channel by placing two pieces of double sided tape on one ITO slide (the ITO coated side) and placed the other slide on top (ITO coated side down). We inserted the solution of active (same concentration as previously described) and passive silica particles (at a concentration of 40 μg/mL) into the channel and sealed it with epoxy. We then placed alligator clips on two ITO slides and applied a voltage of 2.5V, which polarizes the silica particles creating a strong repulsive potential between particles which compose the colloidal monolayer as can be seen in Fig. S13.

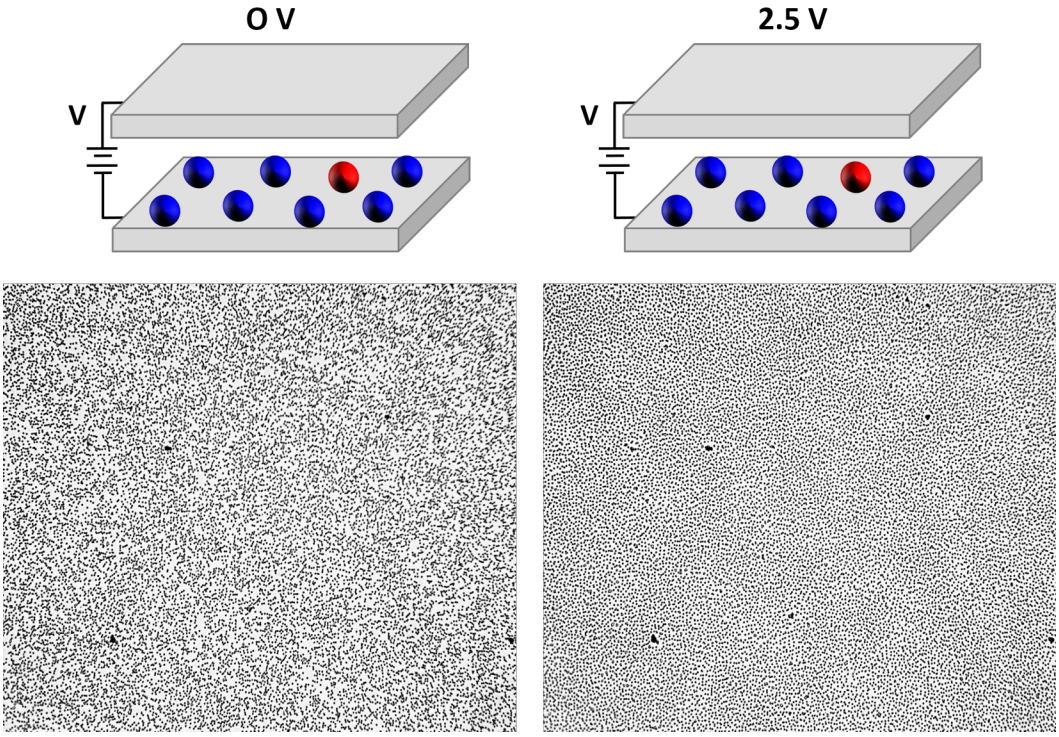

Fig. S 13. Schematic of ITO microfluidic device and experimental snapshots of silica monolayer at applied 0 and 2.5V.

The voltage was maintained at 2.5V for the and spinners were again isolated and the magnetic field was actuated at an angular frequency of 5 Hz as can be seen in Movie S3 and in Fig. S14.

Looking at several spinner trajectories in this passive medium we again see even in this passive medium which has a much lower packing fraction, although it behaves elastically due to this strong repulsive potential applied, the range of attraction is very long range. In this system interaction is observed up to $20D$ apart as seen in Fig. S15.

E. Passive Microrheology Measurements of Passive Medium Elasticity

In order to prove that it is indeed the elastic nature of the passive monolayer that leads to long range spinner attraction we need to be able to quantify the elastic nature of the passive medium. To do this we utilized passive microrheology to obtain this measurement. Passive monolayers of $\phi_A \approx 0.3, 0.5, 0.7$, and the silica monolayer with an applied voltage of 2.5 were created using the protocol previously described. Additionally a monolayer with a packing fraction of $\phi_A \approx 0.9$ was created by following the same protocol for $\phi_A \approx 0.7$ with the exception that the solution was inserted into a channel that was 5 pieces of double sided tape high, instead of the usual 3 pieces. To characterize the visco-elastic nature of these monolayers the passive particles were tracked for a period of approximately 6 minutes. A MatLab program was then used to track the particles, calculate the mean square displacement, fit the data with an exponential function as seen in Fig. S16.

This fit function was then used to calculate the complex modulus by feeding the fit function data into a MatLab function that fits this data with a second-order polynomial function from which the first and second time derivative are computed and from that the complex modulus. The storage modulus (elastic) G' and loss modulus (viscous) G" have been plotted for different monolayer packing fractions as seen in Fig. S17.

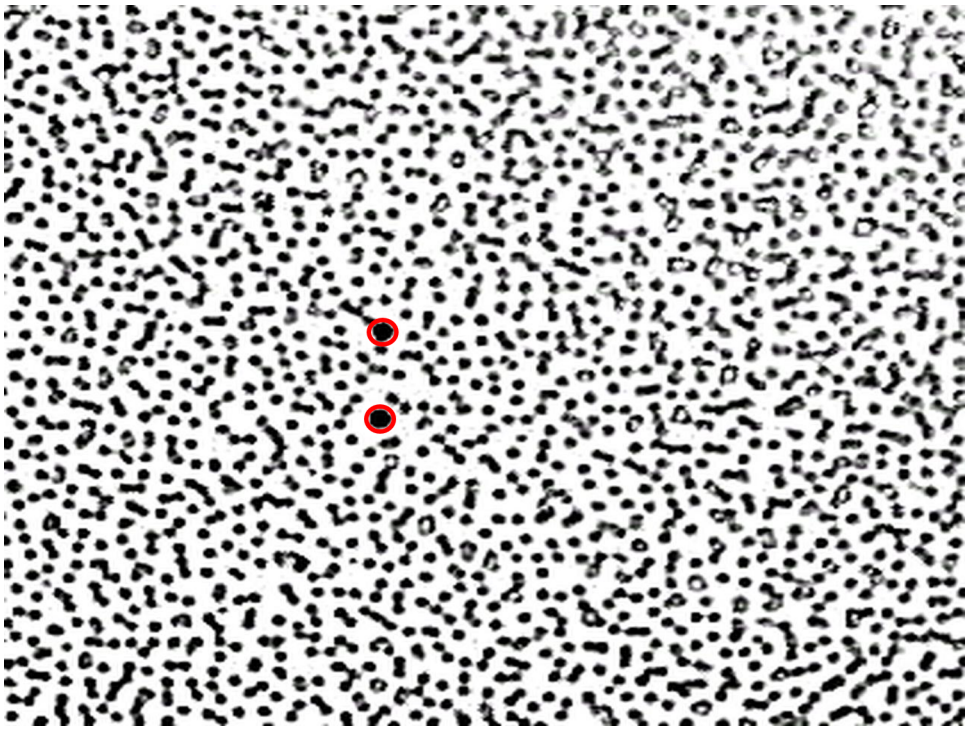

Fig. S 14. Image of spinner attraction in a polarized silica monolayer with an applied voltage of 2.5V. Spinners outlined in red.

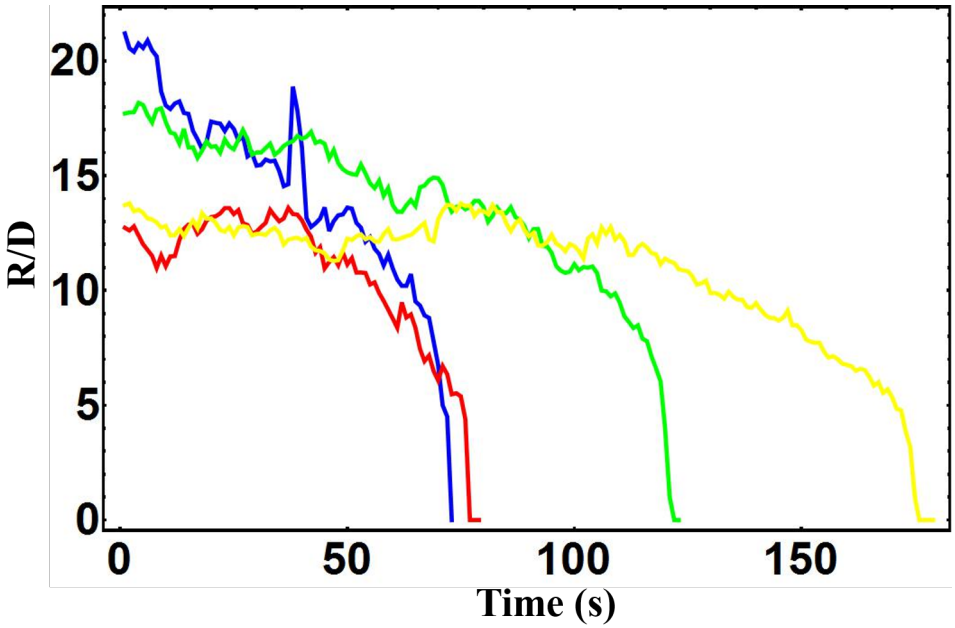

Fig. S 15. Spinner interaction range is extremely long rage, up to $20D$, for this hybrid active-passive system.

The complex modulus measurements illustrate that for polystyrene monolayers at $\phi_A \geq 0.5$ the monolayer behaves elastically for all frequencies or times while for $\phi_A \approx 0.3$ the monolayer behaves elastically at very short times but then transitions to a more viscous medium at longer times. Also for the ITO silica bead monolayer elastically behavior is observed for all frequencies as well. This is a crucial result as it confirms the hypothesis that it is the elastic nature of the passive medium that leads to long-range spinner attraction.

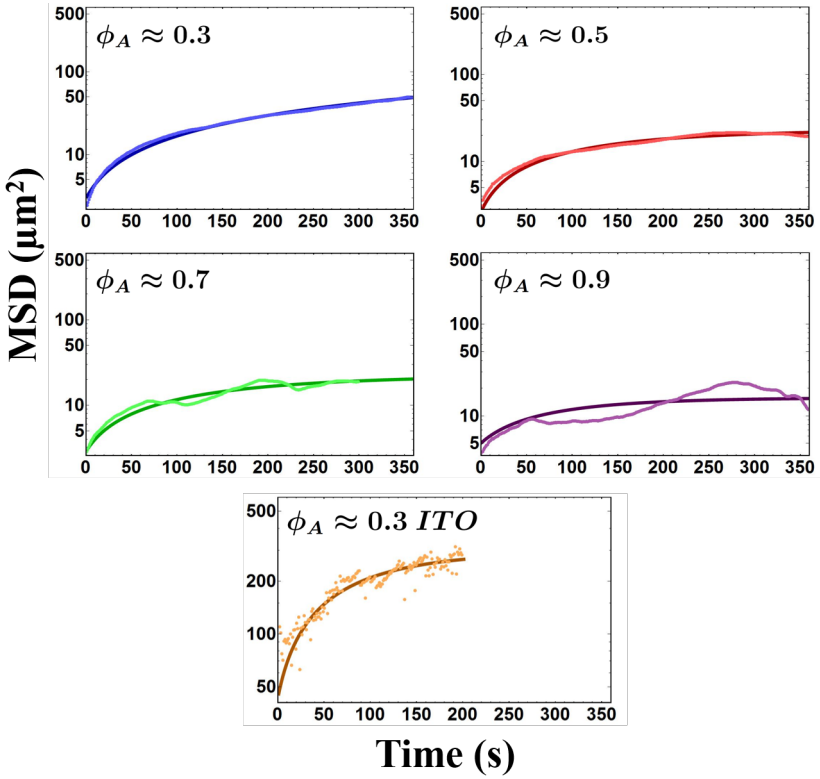

Fig. S 16. Passive monolayer mean square displacement data and exponential function fit for $\phi_A \approx 0.3, 0.5, 0.7, 0.9$, and the ITO silica monolayer $\phi_A \approx 0.3$. The fit is shown in dark and the raw data is the lighter color.

F. Characterizing Fluid Flow of Single Spinners and a Pair of Spinners in the Absence of a Passive Medium

While Lattice-Boltzmann simulations are adept at capturing the hydrodynamic information in a system, we wanted to ensure at least qualitative agreement between the flow fields generated by the spinners. To measure the flow fields around the spinners the same procedure was followed to create the system with spinners in the absence of a passive medium. However, in order to visualize the flow field 1μm tracer polystyrene particles were inserted into the solution. The particles were actuated and the resulting videos were converted into a series of .jpeg images and then analyzed using MATLAB PIVlab 1.35. The resulting flow fields and radial velocity profiles for single particles rotated at 5Hz and 50Hz can be seen in Fig. S18.

It should be noted that there is some error in the analyzing the fluid flow close to the spinners and at distances far away as the tracer velocity doesn't decay to zero. It is clear however that the effective size of the flow field created by the rotating of the spinner increases as the frequency increases. More importantly the effective size of the flow field appears to be somewhat commensurate with the range of spinner interaction found for spinners rotated at 5Hz in the absence of a dense passive medium. The flow field extends almost 2D from the spinners so this helps to explain why we observe interaction between spinners at approximately 3D. The spinners can effectively feel each other through interaction of their flow fields. This can potentially cause small positional fluctuations which then allows the spinners to become close enough so that the magnetic dipole-dipole interaction dominates. However a more interesting question was raised in the manuscript, and in other publications, that active particle aggregation could be attributed to hydrodynamic interactions. The flow field of two isolated spinners, rotated at 5Hz, at different initial distances was also analyzed to investigate how the flow field changes as a function of initial distance, the results can be seen in Fig. S19.

Clearly the flow fields don't interact until the particles are within approximately 3D. At this distance the magnetic dipole-dipole interaction comes into play. Moreover at larger distances, like at 8D, the flow fields don't interact so the spinner aggregation can't be attributed to hydrodynamic forces alone.

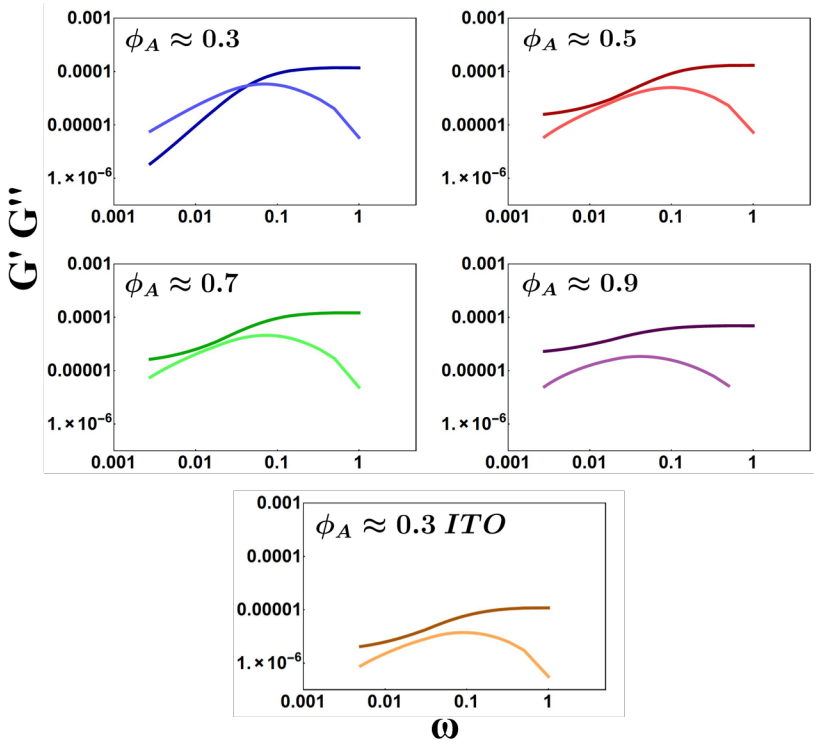

Fig. S 17. Storage and loss modulus as a function of frequency for $\phi_A \approx 0.3, 0.5, 0.7, 0.9$, and the ITO silica monolayer $\phi_A \approx 0.3$. The storage modulus G' is the darker line and the loss modulus G" is the lighter line.

G. Delineating Different Regions In Hybrid Active-Passive Medium: Measuring Corona Size and Rotational Frequency of Passive Particles at the Edge of the Corona

As discussed in the main text there are several regions that we have delineated and given monikers like the bridge and corona. These regions are shown schematically in Fig. S20.

We define the corona as the distance between the spinner and the first shell of particles. The bridge is a more difficult region to measure but it is generally defined as the region of passive particles between the first shell of particles around the spinners. The rest of the passive particles are defined as part of the bulk. The corona is of particular interest and in the main text the process of forming the corona is explained in detail. However, the corona isn't characterized sufficiently within the main text. Of particular interest is the size of the corona and the rotational frequency of the first shell of particles or the particles at the edge of the corona as a function of spinner frequency. To calculate the size of the corona after sufficient actuation period, i.e. enough to form the corona, the average size of the corona was analyzed and plotted as a function of spinner frequency as seen in Fig. S21.

As can be seen the size of the corona expected grows with the spinner frequency however it is interesting to note that at a spinner frequency of 0.5 Hz the difference in corona size is essentially negligible, indicating that at this frequency a corona is unable to form. This can be seen in the embedded videos in the bottom panel. The rotational frequency at which the passive particles rotate around the spinners, actuated at a frequency of 0.5, 1, 3, and 5 Hz, has been analyzed as well and is seen in Fig. S22.

Again we see an almost linear growth in the rotational frequency of the passive particles at the edge of the corona as the spinner frequency increases.

H. Spinner Committor Analysis, Dimer Formation Probabilities, and Investigating Substrate Particle Interactions.

To gain a deeper insight into the emergent spinner attractive interaction and obtain a more quantitative measure of the range of such attraction we preformed a committor analysis of spinner trajectories. The purpose was to determine the probability with which a spinner would attract and form a dimer at different initial distances. Spinner

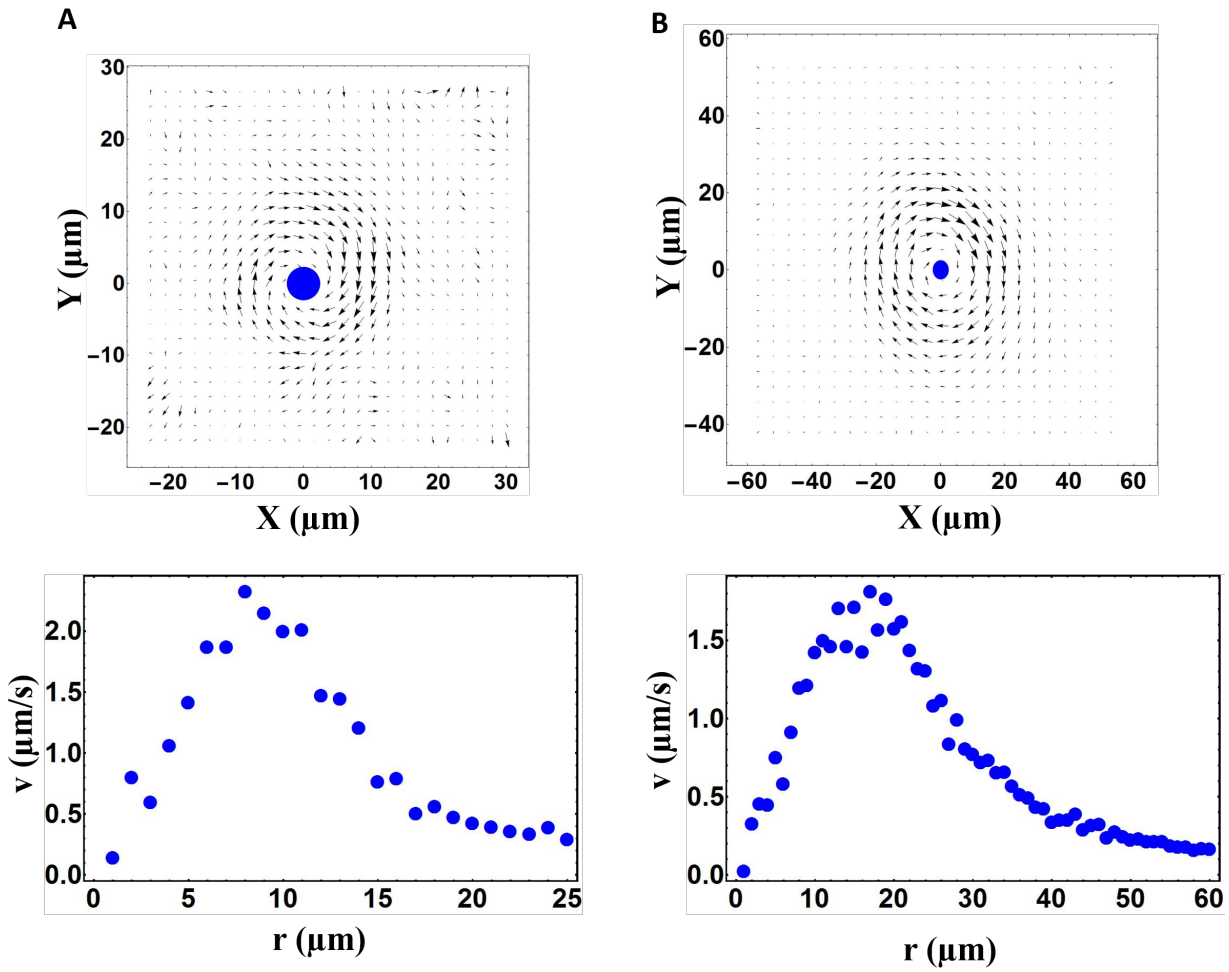

Fig. S 18. The flow field and radial velocity profile measured using 1μm tracer polystyrene beads. A) A single spinner rotating at 5Hz and B) 50Hz

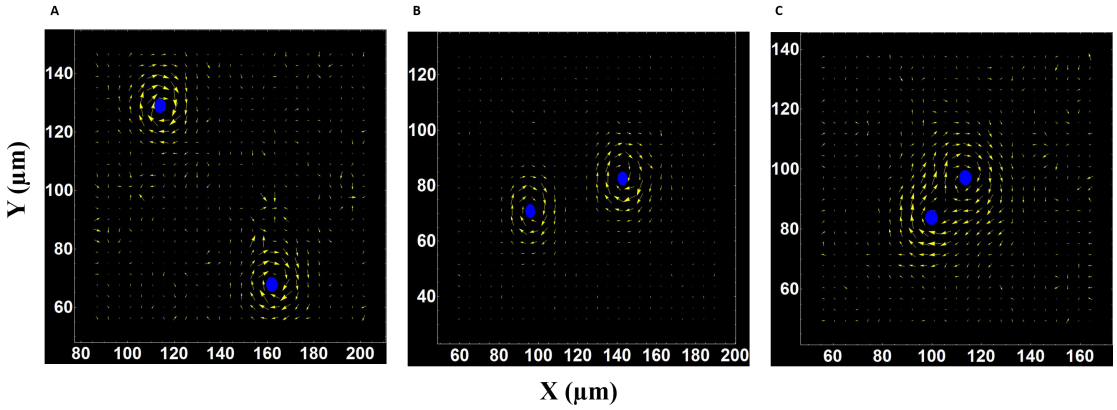

Fig. S 19. The flow field measured using 1μm tracer polystyrene beads of two isolated spinners at three different initial distances A), 78μm B) 49μm, and C) 19μm.

trajectories were binned in time intervals of 5, 10, and 20 seconds. If the average inter-spinner distance decreased that average spinner distance was assigned a value of 1 and if the distance increased it was assigned a value of 0, thus effectively serving as an effective probability of spinner committal to form a dimer. This procedure was repeated

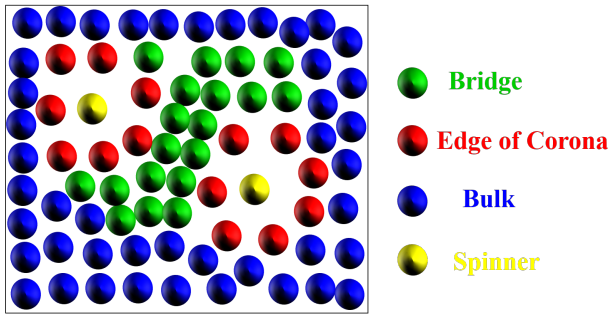

Fig. S 20. Schematic of the different regions in the experimental system referred to in the main text, specifically the bridge (green), bulk (blue), spinner (yellow), and the first shell of passive particles which mark the edge of the corona (red).

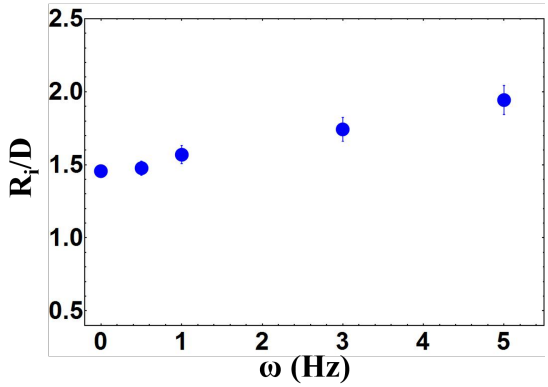

Fig. S 21. The average distance of the first shell of particles from the spinner as a function of frequency, effectively a measure of the size of the corona.

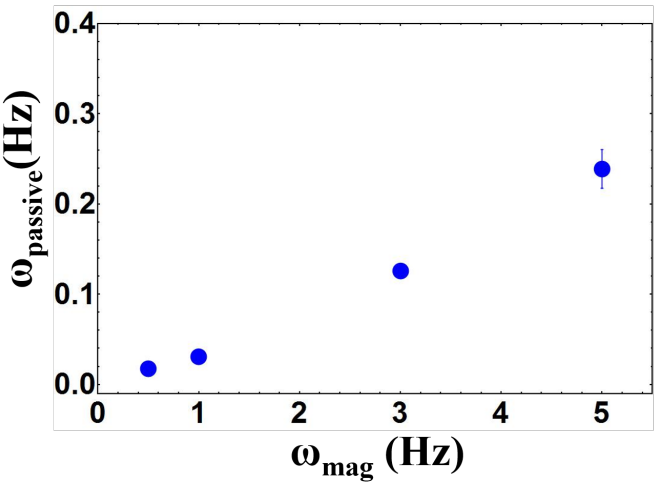

Fig. S 22. The rotational frequency of the passive particles around a spinner which is rotated a frequency of 0.5, 1, 3, and 5 Hz.

for all of the spinner trajectories presented in the range diagrams in Fig.3B, Fig.4, and Fig.5. The spinner distances were partitioned in intervals of one R/D and the spinner distances and committor probabilities were averaged, and example of which can be seen for spinners actuated at an angular frequency of 3Hz in a polystyrene passive monolayer with a packing fraction of $\phi_A = 0.7 \pm 0.1$, in Fig. S23.

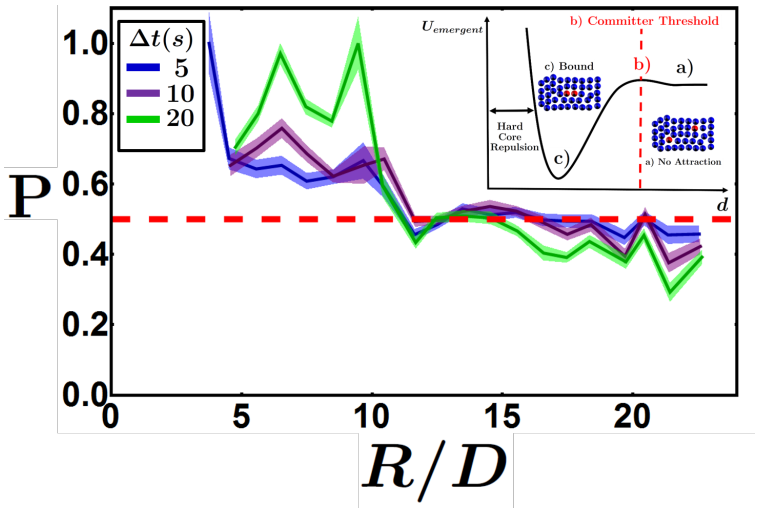

Fig. S 23. Committor probability as a function of normalized spinner distance. Spinner trajectories were binned in time intervals of 5 (blue), 10 (purple) and 20 (green) seconds and the committor probability was calculated. The solid black line represents the committor probability threshold. The committor threshold for pinners actuated at an angular frequency of 5Hz in a polystyrene passive monolayer with a packing fraction of $\phi_A = 0.7 \pm 0.1$ is approximately 11 R/D.

From this figure we calculated the committor threshold distance which is the maximum distance the spinners were committed to forming a dimer. This occurs when the committor probability first drops below a value of 0.5 as this indicates that the spinners were on average repelling more often than attracting. As can be see in Fig. S.23 this value occurs at approximately 11 R/D, the average value where the three curves intersect the solid black line. This same procedure was repeated for all of the experiments represented in the range diagram. These committor threshold values match very well with the range diagrams. It should be noted that this committor threshold value can be a bit of an underestimate as it represents the first time that the committor probability curve dips below 0.5 and one can see there is a small uptick above 0.5 at larger distances in Fig. S.23.

We have also calculated the probability of spinners forming a dimer at different initial starting positions. This is the probability of forming a dimer is simply calculated by taking a ratio of the trajectories that formed a dimer within the experimental timescale over the total number of trajectories for that range. A table of probabilities as a function of monolayer area fraction, frequency in a purely active system and hybrid active-passive system, and spinner actuation protocol can be seen in Fig. S.24.

Additionally we wanted to show that there are no interactions with the particles and the substrate and that such interaction would serve to inhibit the emergent non-equilibrium phenomenon described in this work. To do this inserted passive and active particles coated with streptavidin on a biotin substrate. The biotin-streptavidin bond is the strongest known non-covalent bond with a Kd of approximately 10-15 M-1. What we observed was that the passive particles did not form a monolayer but instead immediately stuck to the surface wherever they sediment as seen in Movie S4 and in Fig. S.25

When the magnetic field is actuated the spinners simply spins in place and are unable to move the passive particles which are now stuck to the surface, thus effectively eliminating emergent spinner attraction.

I. Loading and Measuring the Relaxation Behavior of the Passive Medium

To better understand how the passive medium is loaded, two spinners were isolated and magnetic field was actuated for a period of 1, 2, 5, 10, 30, or 60s and then the direction of the field was reversed and actuated for the same period of time. This procedure was repeated for 5 minutes or until the two spinners formed a dimer. The same sample preparation was used to create the dense colloidal monolayer with a packing fraction of approximately 0.7. The distance between particles was measured as a function of time to measure the attractive force between spinners, as seen in Fig. S26.

A)

Φ_A	Dimer Formation Fraction			
	<10D	<15D	<20D	<40D
0	1/5	1/11	1/13	1/19
0.2-0.34	0/1	0/8	0/13	0/22
0.49-0.58	1/2	2/6	2/6	2/8
>0.61	10/10	13/17	14/19	14/22

Φ_A	Dimer Formation Probability %			
	<10D	<15D	<20D	<40D
0	20	9	8	5
0.2-0.34	0	0	0	0
0.49-0.58	50	33	33	25
>0.61	100	76	74	64

B)

ω(Hz)	Dimer Formation Fraction			
	<10D	<15D	<20D	<40D
0.5	0/6	0/9	0/11	0/17
1	0/3	0/6	0/8	0/15
3	1/2	1/3	1/5	1/12
5	1/5	1/11	1/13	1/19

ω(Hz)	Dimer Formation Probability %			
	<10D	<15D	<20D	<40D
0.5	0	0	0	0
1	0	0	0	0
3	50	33	20	8
5	20	9	8	5

C)

ω(Hz)	Dimer Formation Fraction			
	<10D	<15D	<20D	<40D
0.5	0/2	0/8	0/10	0/19
1	2/4	2/7	2/9	2/15
3	3/3	4/9	4/14	4/16
5	10/10	13/17	14/19	14/22

ω(Hz)	Dimer Formation Probability %			
	<10D	<15D	<20D	<40D
0.5	0	0	0	0
1	50	29	22	13
3	100	44	29	25
5	100	76	74	64

D)

Δt (s)	Dimer Formation Fraction			
	<10D	<15D	<20D	<40D
1	0/7	0/11	0/12	0/12
2	0/7	0/9	0/12	0/12
5	0/5	0/10	0/12	0/12
10	1/2	2/11	2/14	2/14
30	2/2	4/8	4/10	4/10
60	2/2	3/5	3/9	3/10

Δt (s)	Dimer Formation Probability %			
	<10D	<15D	<20D	<40D
1	0	0	0	0
2	0	0	0	0
5	0	0	0	0
10	50	18	14	14
30	100	50	40	40
60	100	60	33	30

Fig. S 24. A)Dimer formation probability and fraction as a function of monolayer area fraction. Spinners were actuated at an angular frequency of 5 Hz. B) Dimer formation probability and fraction as a function of angular frequency for a purely active system. C)Dimer formation probability and fraction as a function of angular frequency for a hybrid active-passive system with a monolayer area fraction $phi_A \approx 0.7$. D)Dimer formation probability and fraction as a function of actuation protocol. Spinners were actuated an angular frequency of 5 Hz in a passive monolayer area fraction $phi_A \approx 0.7$.

At smaller actuation periods there is no attraction between spinners. It is only when the field is actuation for a period of 10-30s that spinner attraction is observed. This result gives us the time it takes to sufficiently load and stress the elastic medium so that spinners can interact. More specifically it tells us the time it takes to form the bridge and compress the bridge as well. While this gives us an idea of the relaxation time of the passive medium we wanted to quantitatively measure some of the elastic properties of the passive medium.

To measure the relaxation behavior of the passive medium an isolated spinner was rotated at frequency of 0.5, 1, 3, and 5Hz in a medium with a packing fraction of approximately 0.7. The field was actuated for approximately 60 seconds and then the field was turned off and the system was allowed to relax back for approximately 5 minutes. The first shell of particles around the spinner were then tracked for this five minute period in order to measure how they relaxed back to their equilibrium position. Only the first shell was considered since these particles can directly measure the relaxation behavior because they are the particles that are directly stressed by the spinners. A torque is exerted on the spinners by the magnetic field and the spinners exert a force on the surrounding fluid which then collides with the passive particles in the first shell so by measuring how the first shell relaxes back we can extract the spring constant of the elastic medium. The first shell was tracked for the entire relaxation period and the time it took for the passive particles to relax back to their initial position, τ_{relax} is plotted as a function of field frequency is seen in Fig. S27.

As anticipated the relaxation time increases as the angular frequency of the magnetic field increases. With this relaxation time we can then calculate the velocity of the passive particles as it travels back to its initial condition and plug this into the Stokes equation in order to derive the the spring constant of the passive medium. We find that the spring constant decays as the angular frequency of the applied field increases.

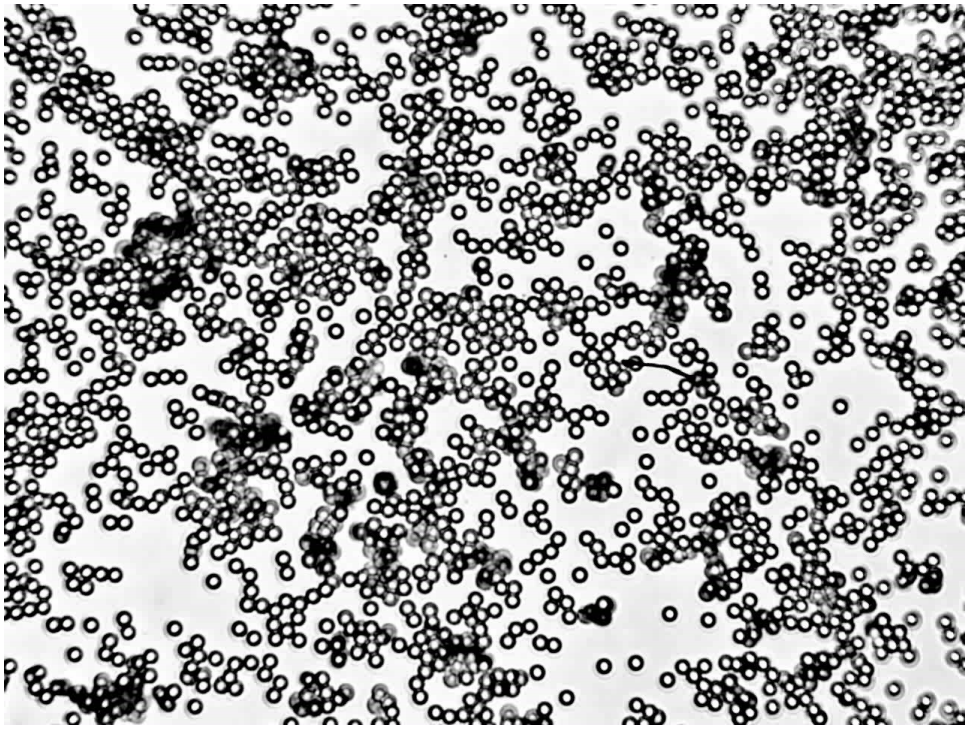

Fig. S 25. Experimental snapshot of biotin substrate and passive particles and spinners coated in streptavidin.

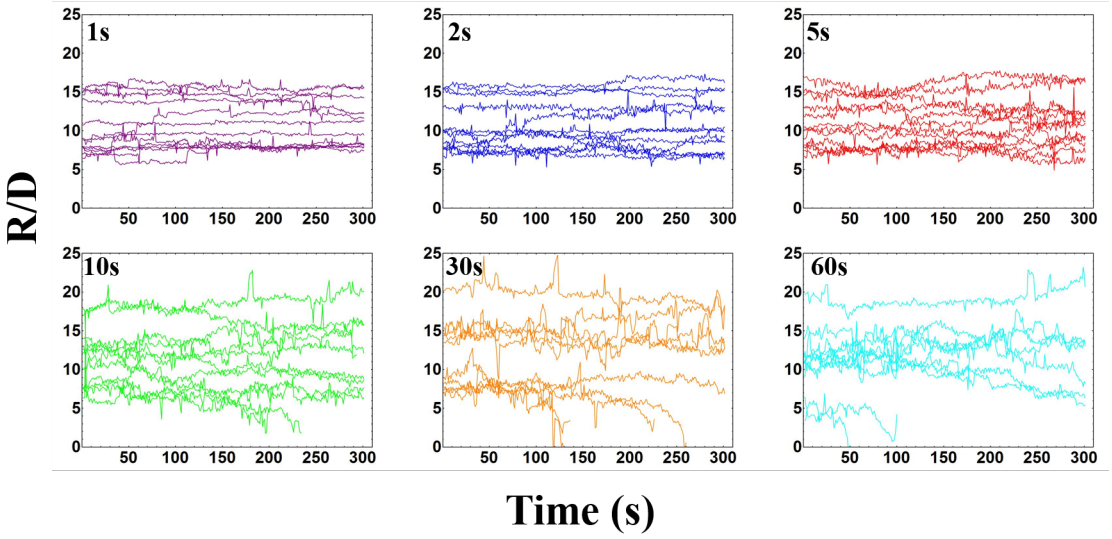

Fig. S 26. The trajectories of the distances between the spinners show that there is no long range attractive force until the passive medium is loaded for approximately 10-30s.

J. Simulation Results

We have also carried out simulations of the system studied here. Our simulation model considers explicitly the fluid by means of a Lattice-Boltzmann (LB) fluid [1], which couples to spherical solid objects following the bounce-back rule and imposing no-slip boundary conditions at their surfaces. More specifically, we have implemented the ALD method [2]. The LB fluid parameters considered here were density $\rho = 1$, kinematic viscosity $\nu = 1/6$ and temperature $k_B T = 210^{-5}$. The simulation box represents a channel bounded in the z direction by a no-slip walls, while periodic

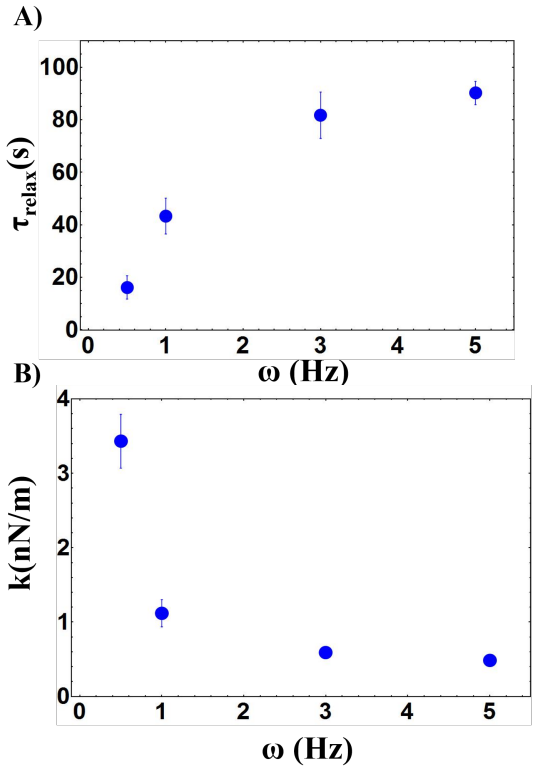

Fig. S 27. Measuring elastic behavior of the corona. A) The relaxation time, τ_{relax}, grows as a function of field angular frequency. B) The spring constant decays as the angular frequency of the magnetic field increases.

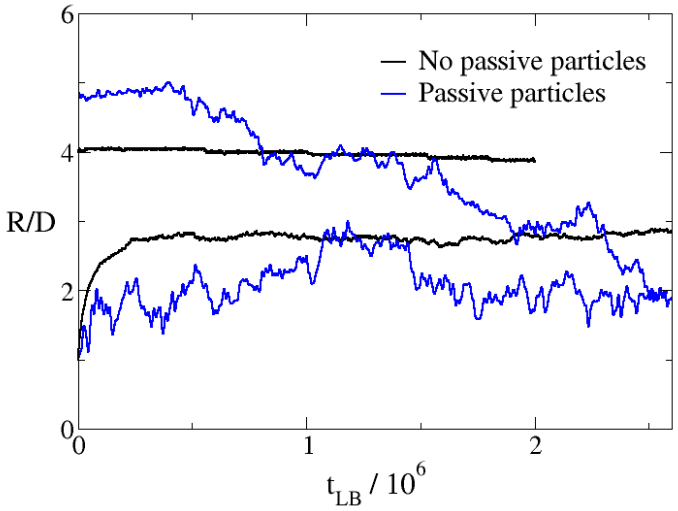

Fig. S 28. Time evolution of the distance between two spinners at Re = 0.84 in a viscous fluid (black lines) and embedded in passive monolayers of $\phi_A = 0.8$ (blue lines).

boundary conditions are applied in the x and y directions. Accordingly, the simulation box is discretized in three dimensional grids of $N_x \times N_y \times N_z = 214 \times 214 \times 30$, where we have set the grid spacing, Δx, and the LB time step, Δt_{LB}, to unity. The particles, of diameter D=12Δx, are described as real solid objects interacting through a hard-sphere potential [3] and subjected to a gravitational force, $F_G = 0.005$, which causes the particles to sediment on the bottom of the channel. The activity of the spinners was achieved by imposing an external torque around the

z-axis to make the particles' Reynolds number ($Re = \omega D^2 \rho/\eta$) Re=0.84. Since we are interested in the passive-media induced interactions between the spinners, in this simulation model we have neglected the dipole-dipole interactions between them.

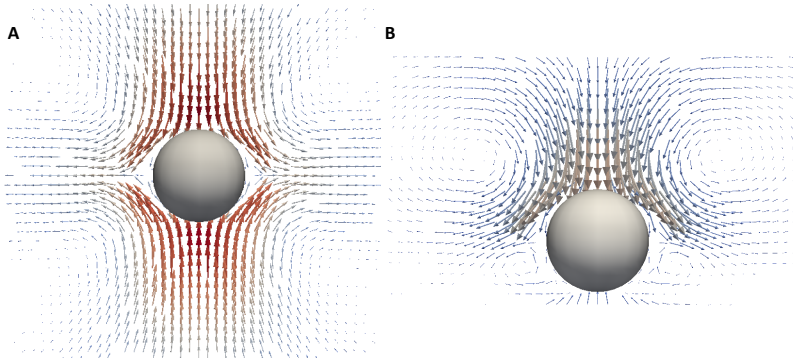

Fig. S 29. Secondary flow in the xz plane generated by a spinner rotating about the z-axis in bulk (A) and close to a wall (B)

.

We have performed numerical simulations of the spinners initially positioned at different distances in two different scenarios: i) Pairs of spinners in a viscous fluid (i.e. without passive particles) and ii) pairs of spinners embedded in dense passive monolayers. The simulation trajectories obtained from these situations are presented in Fig. 28. We observe that the spinners experience a repulsive interaction when suspended in a viscous fluid, while the interaction is attractive when embedded in a dense passive matrix. The repulsive interaction between spinners in the absence of passive particles originates from the secondary flows generated by the spinners [4]. In the experiments, this hydrodynamic repulsion is masked by the strong dipole-dipole interaction; however, it is the responsible for the formation of the corona and the subsequent compression of the monolayer.

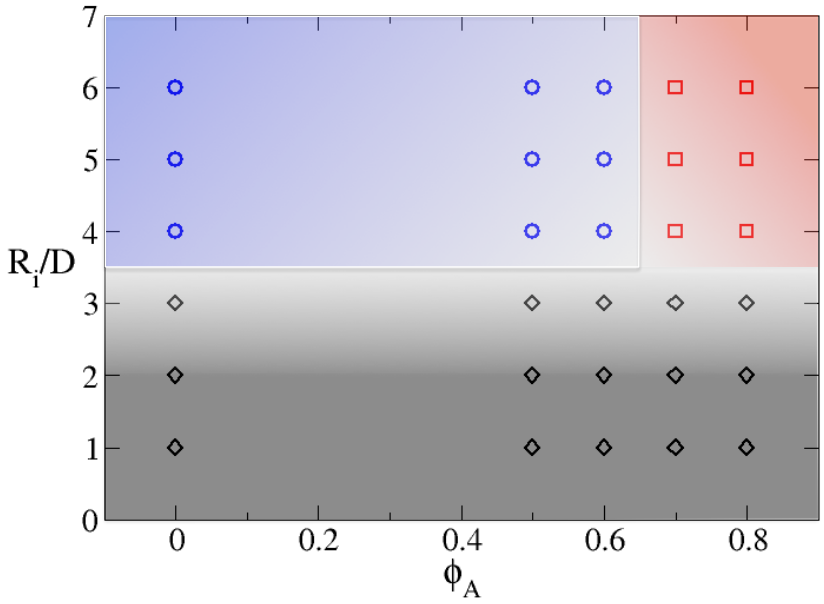

Fig. S 30. Range of the interaction as a function of the area fraction of passive monolayers obtained from the numerical simulations. The different symbols represents: i) no interaction (blue circles), ii) hydrodynamic repulsion (black diamonds) and iii) attraction (red squares).

A spinner suspended on a viscous fluid and rotating around the z-axis at a frequency ω generates a rotating fluid flow, which velocity field at Re = 0 is given by

$$u(r) = \frac{\tau}{8\pi\eta r^3}\hat{z} \times \mathbf{r} \tag{2}$$

where $\mathbf{r}$ is the position of the fluid from the center of the particle, τ is the torque acting on the particle and η is the fluid viscosity. At small but finite Reynolds numbers, inertial terms generate additional forces on the particles due to the momentum of the fluid. Under these conditions, the fluid velocity profile generated by a rotating sphere (Eq. 2) needs to be corrected to include these inertial terms, which generate a so-called secondary flow, as shown in Fig. 29. Because of the centrifugal force effect, the fluid is pulled in toward the poles and expelled from the equator, which generates a secondary flow on the zx-plane.

Therefore, the secondary flows besides being the responsible of the formation of the corona because of the repulsion of the neighboring passive particles. The role of these secondary flows is thus crucial for this interaction because they provide the compression strain on the bridge required to load the system.

In the presence of the passive particles the mechanical properties of the medium changes from viscous to elastic and the direction of the forces reverses, thereby resulting in an effective attractive interaction between the active objects. To corroborate that it is indeed the change in the mechanical properties of the medium that is responsible for the effective attraction between the spinners in dense passive monolayers, we performed simulations of spinner pairs in monolayers at different area fractions. From those simulations we built a *range diagram*, analogous to the experimental one in Fig. 3B, presented in Fig. 30. In agreement with the experiments, we observe that there is a threshold in the passive-mediated interaction for $\phi_A < 0.7$, which coincides with the change from a solid-like to a viscous material, as shown in Fig. 31.

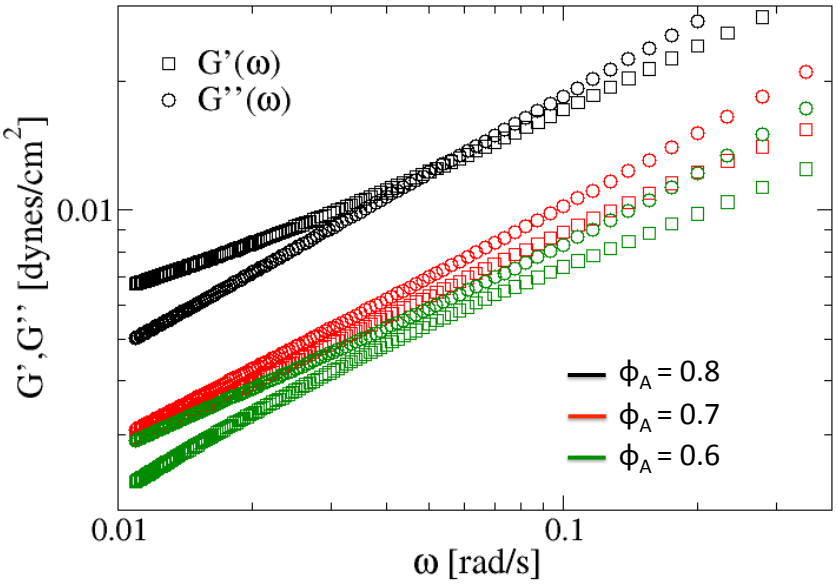

Fig. S 31. Frequency-dependent storage modulus (squares), $G'(\omega)$, and loss modulus (circles), $G''(\omega)$, for passive monolayers at area fractions of $\phi_A = 0.8$ (black symbols), $\phi_A = 0.7$ (red symbols) and $\phi_A = 0.6$ (green symbols). Obtained from the Mean Square Displacements (MSD) of the passive particles in the different monolayers in the absence of spinners.

[1] B Dünweg and A. Ladd. Lattice Boltzmann Simulations of Soft Matter Systems. *Adv Polym Sci*, pages 1–78, November 2008.
[2] E-Jiang Ding and C. K. Aidun. Extension of the lattice-Boltzmann method for direct simulation of suspended particles near contact. *Journal of Statistical Physics*, 112:685, August 2003.
[3] J Jover, A J Haslam, A Galindo, G Jackson, and E A Muller. Pseudo hard-sphere potential for use in continuous molecular-dynamics simulation of spherical and chain molecules. *J. Chem. Phys.*, 137(14):144505, 2012.
[4] Juan L Aragones, Joshua P. Steimel, and A Alexander-Katz. *arXiv:1512.02562*, 2015.